



**HAL**  
open science

## Cyclic behaviour modelling of GFRP adhesive connections by an imperfect soft interface model with damage evolution

Marco Lamberti, Aurelien Maurel-Pantel, Frédéric Lebon, Francesco Ascione

► **To cite this version:**

Marco Lamberti, Aurelien Maurel-Pantel, Frédéric Lebon, Francesco Ascione. Cyclic behaviour modelling of GFRP adhesive connections by an imperfect soft interface model with damage evolution. *Composite Structures*, 2022, 279, pp.114741. 10.1016/j.compstruct.2021.114741 . hal-03406895

**HAL Id: hal-03406895**

**<https://hal.science/hal-03406895>**

Submitted on 13 Dec 2021

**HAL** is a multi-disciplinary open access archive for the deposit and dissemination of scientific research documents, whether they are published or not. The documents may come from teaching and research institutions in France or abroad, or from public or private research centers.

L'archive ouverte pluridisciplinaire **HAL**, est destinée au dépôt et à la diffusion de documents scientifiques de niveau recherche, publiés ou non, émanant des établissements d'enseignement et de recherche français ou étrangers, des laboratoires publics ou privés.



Distributed under a Creative Commons Attribution - NonCommercial - NoDerivatives 4.0 International License



1  
2  
3  
4  
5  
6  
7  
8  
9  
10  
11  
12  
13  
14  
15  
16  
17  
18  
19  
20  
21  
22  
23  
24  
25  
26  
27  
28  
29  
30  
31  
32  
33  
34  
35  
36  
37  
38  
39  
40  
41  
42  
43  
44

## 1. Introduction

In the last decades, fibre reinforced material (FRP) have become more attractive as alternative to traditional construction materials thanks to their excellent mechanical properties such as high tensile strength and resistance to aggressive environments, high strength to weight ratio, simple and rapid installation time [1-5].

The availability on the market of continuous FRP profiles with constant cross-section such as hollow sections, angle, I-beams and channels, suitable for construction of frame structure, has been guaranteed during the years by the pultrusion process.

In this framework, one of the most promising application in the field of complex structure, is the realization of hollow column to built-up beam connection by using structural adhesives, becoming a valid alternative to the classical bolted connection.

Nowadays, in the civil engineering field, the connections in FRP structures are commonly made using bolted connections excluding a priori the bonding technique. Some FRP profiles manufacturers [6] and design guidelines [7] stipulates that bonded connections should not be allowed for primary load bearing components being the lack of knowledge about and experience with their performance the main reason for their prohibition [6].

Indeed, the most important feature that characterizes the adhesive connections is the absence of holes: the stresses are more uniformly distributed over the bonded surface avoiding the presence of high stress concentration that could damage the fibres and increase the risk of moisture penetration in members.

This lead to consider these type's connections particularly suitable for the construction of structures in aggressive environments, such as the wind installations in the offshore structures in marine environment.

In this case, the performance of adhesive connections can be influenced by the presence of leading causes of degradation, such as vibrations (due to the waves) represents certainly an aspect to be deeply investigated.

Recently, to improve the confidence that nowadays limits the use of this technology, several authors have undertaken experimental and numerical investigations.

Encouraging results, both from experimental and numerical point of view on the beam-column adhesive connections made in GFRP materials have been obtained by some authors [9-13].

To investigate the strength, stiffness and fatigue strength of adhesive connections, the response under quasi-static, cycling and fatigue loading have been tested. Furthermore, the connection response under static load has been compared with the behaviour of an analogous bolted connection to demonstrate the better overall performance of the former.

Therefore, it born the need to develop a methodology based on an imperfect interface approach [13] to improve the knowledge of the behaviour of GFRP structures characterized by such connections.

In this paper, a predictive numerical model of the cyclic behaviour has been presented and successfully compared to experimental results.

The model is derived by an asymptotic analysis, due to the thickness of the adhesive layer, of a composite structure made of two elastic solids bonded together by a third thin one, which has a nonlinear behaviour. The adhesive is micro cracked by adopting a Kachanov-type assumption [14-15]. More in detail, the Kachanov's theory considers an adhesive layer microcracked characterized

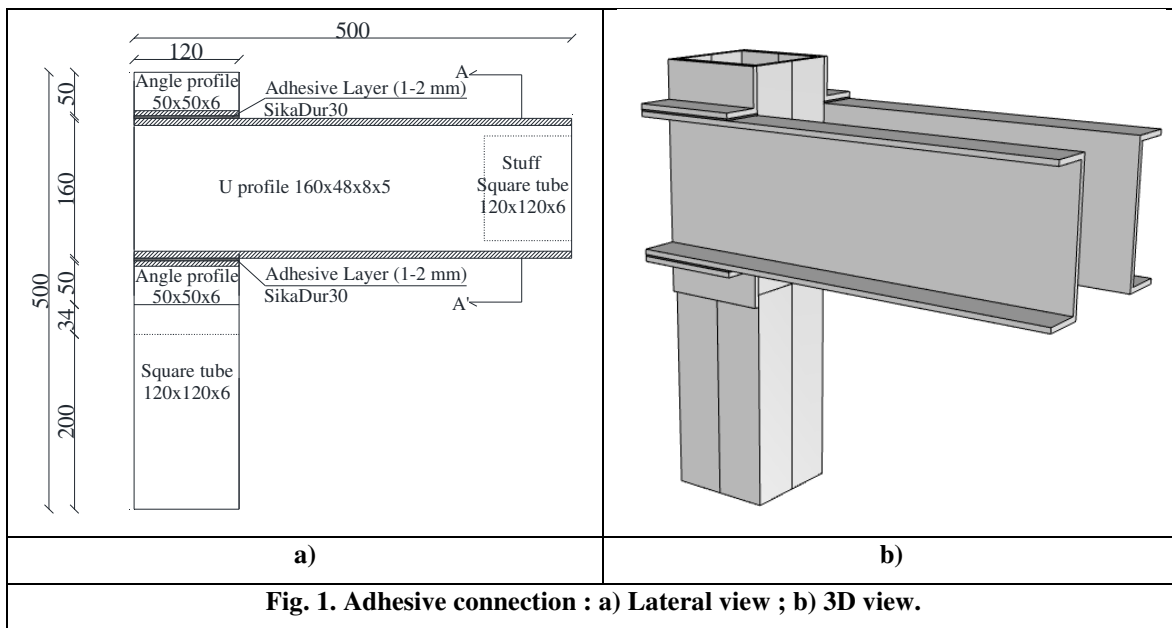
1 by the following assumptions: there is no interaction between the cracks, the stress vector along the  
 2 crack is assumed constant, and in the stress field, the effect of crack edge is ignored. The present  
 3 model is able to take into account several adhesive parameters such as thickness, porosity, presence  
 4 of an initial damage and to describe the damage evolution.  
 5 In order to quantify the mechanical parameters such as stiffness of adhesive, initial damage and  
 6 damage evolution, some experimental tests on adhesive layer in cyclic load condition have been  
 7 undertaken. The experimental evidence underlines the progressive evolution on the damage at varying  
 8 of cycle load. Based on the experimental results, the interface model is enhanced.  
 9 Finally, we have implemented the model in a finite element software and demonstrated its powerful  
 10 comparing numerical and experimental results.

11

## 12 2. GFRP hollow column to built-up beam adhesive connection: experimental test

13

14 In a previous research program deeply described in [11], some of authors have experimentally  
 15 investigated the behaviour of full scale GFRP connections under static and cyclic load. The  
 16 investigated connections join a tubular column made of a commercially available hollow GFRP  
 17 profile with square cross section (120x120x6 mm) and two U-profiles (160x48x8x5 mm) ranged  
 18 together in the form of a built-up beam. Both the beam and the column are 500 mm long. The  
 19 members were joined together using an epoxy-based adhesive available on the market called SikaDur  
 20 30 [16]. Four angle profiles (50x50x6mm) were positioned at the bottom and the top of the U-profiles  
 21 with the scope of maximise the bonded surface area. The adhesive layer was 1-2 mm thick.  
 22 The adhesive connections, object of the present numerical investigation, are depicted in Fig. 1.  
 23



24

25 The specimens have been originally designated as AC,*i* where AC stands for Adhesive Connection  
 26 while *i* represents the *i*-th specimen.

1 Each specimen was loaded by a line load applied near the free end of its built-up beam by means of  
 2 a rigid steel arm clamped to the testing machine, at 420 mm from the axis of the column. The column  
 3 was inserted into a steel jacket filling the small gaps by steel shims; therefore, it can be assumed as  
 4 fixed at its basis.

5 The specimens were subjected to three loading regimes: quasi-static, cyclic and fatigue.  
 6 The static test was performed in displacement control at a rate of 2 mm/s, the load monotonically  
 7 increasing quasi-static load up to failure. In the second regime the specimens were subject to a high  
 8 amplitude loading-unloading cyclic load (50 % of the maximum load for three different number of  
 9 cycles, 400, 800 and 1200) and finally in the third regime the specimens were subject to variable  
 10 amplitude fatigue load (50%, 75%, 85%, and 95% of the maximum load for a fixed number of cycles  
 11 equal to 60).

12 From the experimental evidence it is noted the static tests lead to a response practically linear with  
 13 slight deviation from linearity near the failure load (Figure 2).  
 14

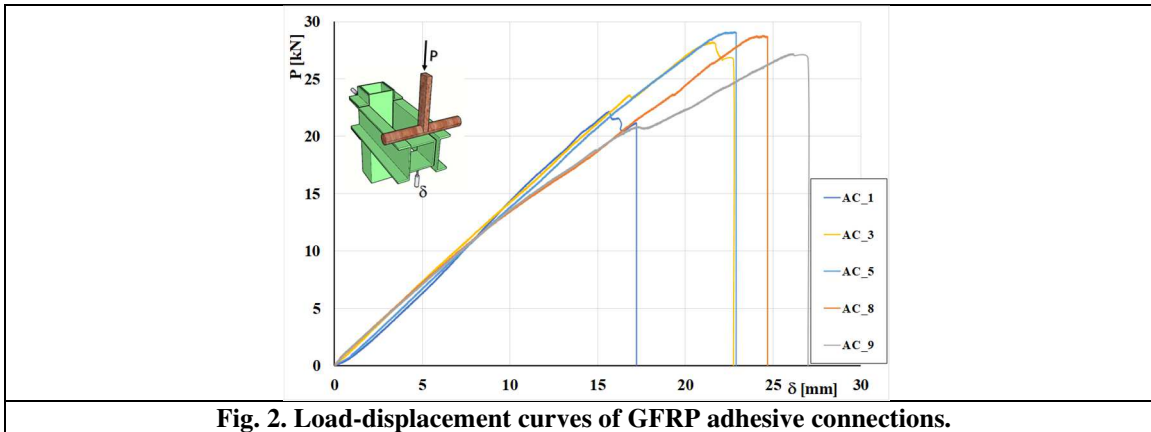


**Fig. 2. Load-displacement curves of GFRP adhesive connections.**

15  
 16 The results of the cyclic load tests on the adhesive connections subjected to 400, 800 and 1200  
 17 loading-unloading cycles are presented in Figures 3, 4 and 5, respectively.

18 For the sake of clarity, only curves for the first loading cycle and the last unloading cycle of each  
 19 specimen are shown. To avoid crowding and facilitate the current discussion, the graphs for the  
 20 intermediate cycles are not plotted but they follow a similar trend and fall within the first loading and  
 21 the last unloading curve.  
 22

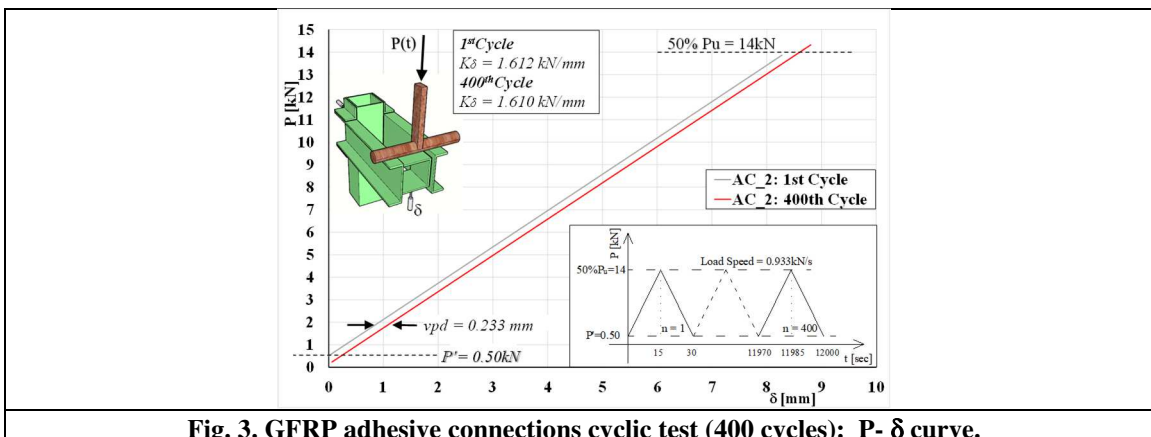


**Fig. 3. GFRP adhesive connections cyclic test (400 cycles): P- δ curve.**

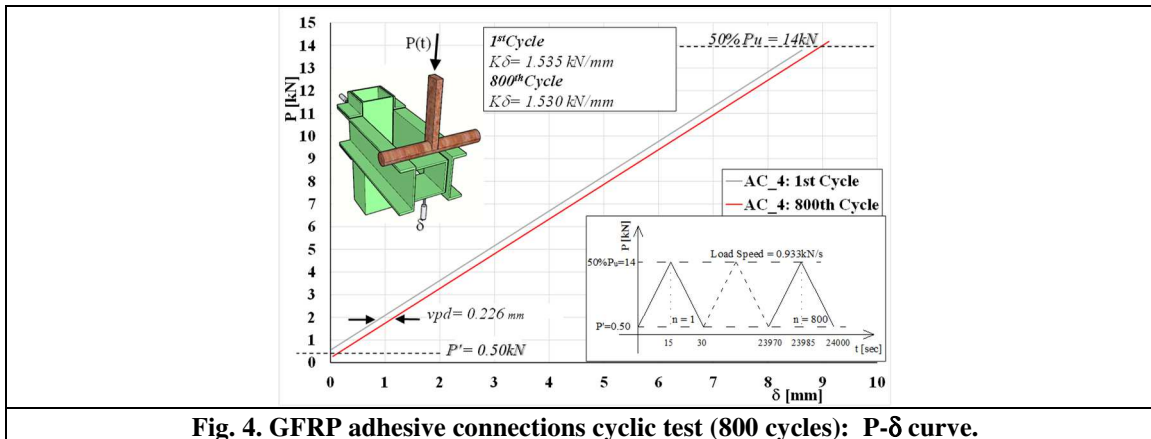


Fig. 4. GFRP adhesive connections cyclic test (800 cycles): P- $\delta$  curve.

1

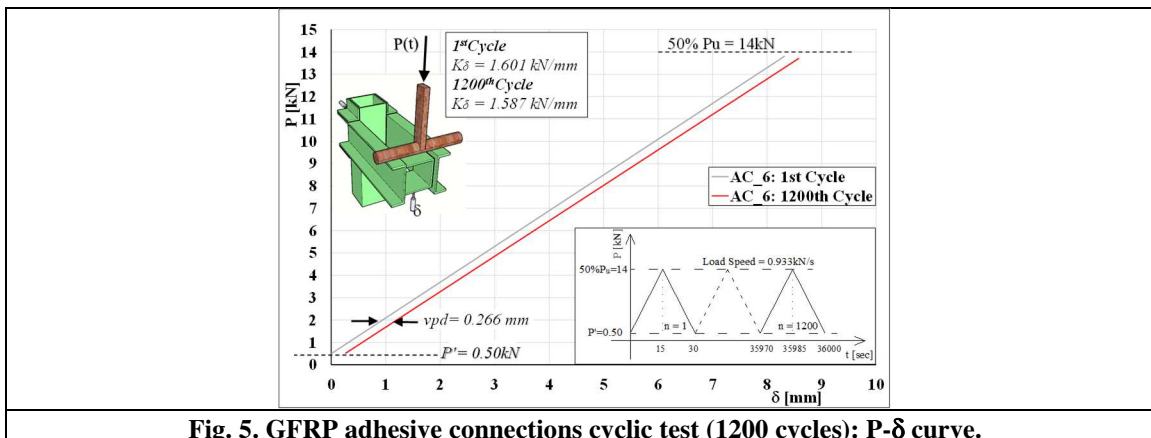


Fig. 5. GFRP adhesive connections cyclic test (1200 cycles): P- $\delta$  curve.

2

3 Finally, the results with reference to the adhesive connections subjected to fatigue loading involving  
 4 loading-unloading with increasing load amplitude after each 60 load cycles are depicted in Figure 6.  
 5 Once again, the first cycle loading curve and the last cycle unloading curve corresponding to each  
 6 load amplitude are shown. Notice that the first cycle loading curve for the 2<sup>nd</sup>, 3<sup>rd</sup> and 4<sup>th</sup>  
 7 load amplitudes coincides with the last cycle unloading curve of the preceding load amplitude.  
 8 These figures show that up to nearly the end of the third load amplitude, the connections suffered  
 9 only minor reduction in stiffness but after the application of the load with the 4<sup>th</sup> amplitude, the  
 10 stiffness dropped substantially. This reduction was instigated by the appearance of cracks in the  
 11 adhesive layer between the column face and the lower shelf angle towards the end of the 3<sup>rd</sup> load  
 12 amplitude cycles and the subsequent extension and opening of the cracks under the load with the 4<sup>th</sup>  
 13 amplitude. As a result of these cracks, specimens failed after few cycles of the load with the 4<sup>th</sup>  
 14 amplitude. It is, however, interesting to notice that despite the appearance of the cracks, these  
 15 specimens remained linear elastic throughout the loading and unloading cycles up to failure.  
 16

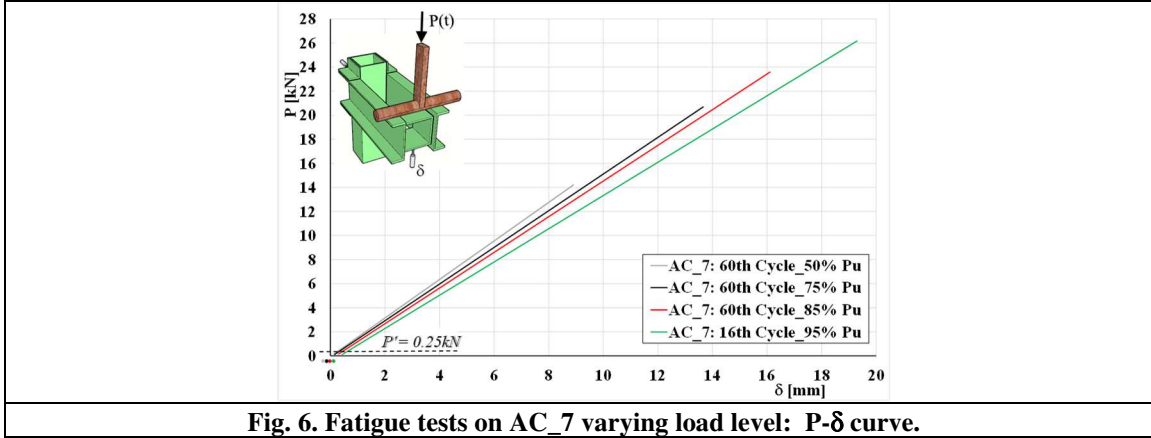


Fig. 6. Fatigue tests on AC\_7 varying load level: P-δ curve.

1

2

3

### 3. Imperfect Interface Model

4

5 The proposed imperfect interface model has been developed coupling the homogenization technique  
 6 and the asymptotic approach within the small perturbation framework [17]-[21]. The model considers  
 7 unilateral contact condition and includes the damage development of the interface.

8 Following the approach introduced in [22]-[23], the thin adhesive interphase placed between the two  
 9 adherents is considered to be a microcracked material subject to a degradation process.

10 In detail, the real microstructure of the adhesive comprises several microcracks families with  
 11 randomly distributed lengths and orientations.

12 Furthermore, the idealized microcracked adhesive layer is obtained by adopting a Kachanov-type  
 13 homogenization technique [14]-[15] based on the Eshelby's problem. The homogenized material is  
 14 used to model the thin adhesive interphase of thickness  $\varepsilon$  between the two adherents.

15 Within this non-interactive approximation framework [15], the family of microcracks with parallel  
 16 orientation to the bonding plate is withheld representative of the macroscale behaviour of the adhesive  
 17 by means of the equivalent length of microcracks family denoted as  $l$ .

18 The effective mechanical properties depend on the microcracks density  $\rho$  which is function of the  
 19 length of cracks  $l$  and the volume  $V$  of the representative elastic domain as reported in Equation (1).

20

$\rho = \frac{l^3}{V}$	(1)
------------------------	-----

21

22 It is important to underline that the crack density  $\rho$  can evolve in the time representing thus a damage  
 23 parameter. In fact, an evolution law can be introduced on the parameter  $l$ .

24 Consequently, the variation in time of  $l$  can be associated to a pseudo-potential dissipation  $\phi$  given  
 25 by the sum of a quadratic term (rate-dependent) and a positively homogeneous functional (rate-  
 26 independent) as reported in Equation (2).

27

$\phi(i) = \frac{1}{2}\eta i^2 + I_{[0, \infty[}(i)$	(2)
--	-----

1  
2 where  $\eta$  is a positive viscosity parameter function of the thickness of the adhesive layer and  $I_B$  denotes  
3 the indicator function of a set B, i.e.  $I_B = 0$  if  $x \in B$  and  $I_B = \infty$  otherwise. Furthermore, the term  
4  $I_{]0,\infty[}$  forces the crack length to assume non-negative values, in this way the crack length can only  
5 increase making irreversible the degradation process of the glue.  
6 According to the Kachanov-type material, the adhesive is considered as a soft material.  
7 However, in the current model, to impose unilateral contact (non-penetration condition) in the  
8 asymptotic expansion, the glue is considered as a soft material only in traction.  
9 The bonding presence between the interphase and the adherents is considered perfect to guarantee the  
10 continuity in the interface separation and stress vector.  
11 Using matching asymptotic expansions, the interphase volume of the glue is replaced by an interface  
12  $S$  of normal unit  $n$ . This permits to obtain a relationship the following equations across the surface  $S$ .  
13

$\sigma n = K(l)[u]_+ + \tau n$ on $S$	(3)
$\tau[u].n = 0, \tau \leq 0, [u].n \geq 0$ on $S$	(4)
$\bar{\eta}l = \left( \bar{\omega} - \frac{1}{2} K_{,l}(l)[u]_+.[u]_+ \right)_+$ on $S$	(5)

14  
15 More in detail,  $[u]$  denotes the jump in the displacement field across the interface  $S$  and  $\sigma$  the Cauchy  
16 stress tensor.  
17 Where  $(\cdot)_{,l}$  denotes the partial derivate in  $l$ ,  $(\cdot)_+$  is the positive part of a function, i.e.  $[u]_+ = [u]$  if  
18  $[u].n \geq 0$ ,  $[u]_+ = [u] - [u].n$  if  $[u].n \leq 0$ . The parameter  $\bar{\eta}$  is the limit of  $\eta\varepsilon$  for  $\varepsilon \rightarrow 0$  as well as  $\bar{\omega}$   
19 is the limit of  $\omega\varepsilon$ . Further information of the asymptotic expansion can be found in [17].  
20 The interface constitutive law described in Equation (3-5) and in Fig. 7 represents a spring-like  
21 interface model with a non-linear damage evolution. In fact, as aforementioned, Equation (5)  
22 represents the evolution of the parameter  $l$  by a simple derivation of a quadratic pseudo-potential of  
23 dissipation, the coefficient  $\omega$  is a negative parameter similar to the Dupré's energy.  
24 Furthermore, the damage process starts only if the elastic work is greater than a given value  
25  $\omega$  function of the thickness of the glue.  
26 Finally,  $K$  is the stiffness tensor of the interface that takes in memory the initial features of the  
27 interphase such as geometry and mechanical properties.  
28 The homogenization technique and the asymptotic approach leads to obtain the following expression  
29 of the tangential and normal stiffness for a bonding interface:  
30

$K_N(l) = \frac{3E_T S}{16l^3(1-\nu^2)}$	(6a)
$K_T(l) = \frac{3E_T S(2-\nu)}{32l^3(1-\nu^2)}$	(6b)

1  
 2 where  $E_T$  is the Young modulus of the adhesive and  $\nu$  its Poisson ratio.

3 How is possible to note, the behaviour of adhesive layer is described by an interface model where the  
 4 stiffness of the glue is function of the variable damage.  
 5

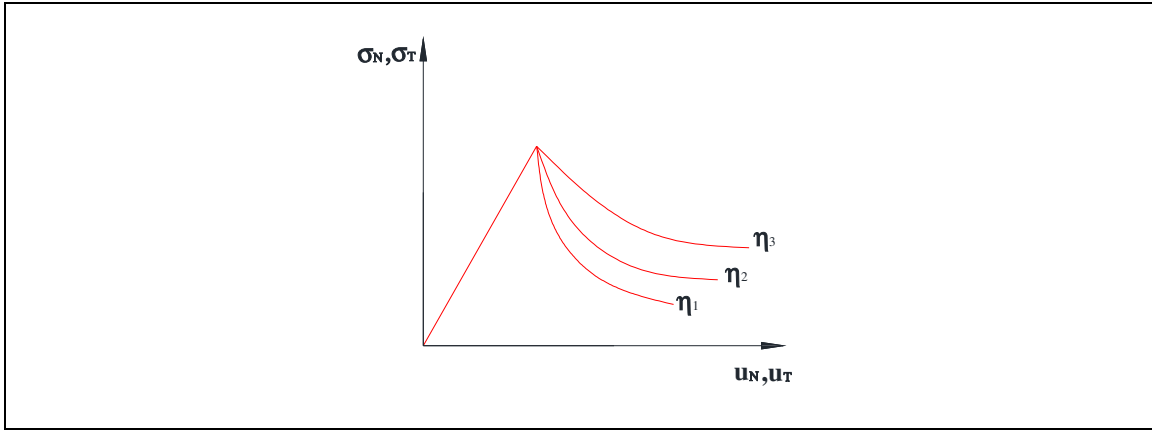


Fig. 7. Interface constitutive law for normal and tangential stress component at varying of  $\eta$ .

6  
 7  
 8 **4. Characterization of the cyclic behaviour of the Adhesive**

9  
 10 In order to calibrate the damage parameters of the interface model aforementioned according with  
 11 Kachanov's theory, several experimental tests, designed ad hoc, have been conducted at Mechanical  
 12 and Acoustics Laboratory (LMA) in Marseille (France).

13 The specimens (Fig.8) have been constituted by two cylindrical parts in aluminium with diameter  
 14 equal to 18 mm. The total length of each cylindrical specimen is 120 mm.

15 Three different adhesive thicknesses have been tested, equal to 1, 5 and 10 mm, respectively. As a  
 16 consequence the specimens are designated as  $At,i$  where  $At$  stands for Adhesive thickness while  $i$   
 17 represents the value of thickness.

18 The epoxy-based adhesive used to connect each other the elements in the current experimental  
 19 investigation was Sikadur-30 [16].

20 The mechanical properties of Aluminium and adhesive are summarized in Table 1.

21  
 22 **Table 1. Mechanical Properties of Aluminium**

	Value
Young's Modulus, $E_A$	70.000 MPa
Poisson's ratio, $\nu_A$	0.2

23  
 24 **Table 2. Mechanical Properties of epoxy adhesive (SikaDur-30)**

	Value
Young's Modulus in compression, $E_C$	9.600 MPa
Young's Modulus in tension, $E_T$	11.200 MPa

Compressive Strength, $\sigma_c$	70-80 MPa (at 15°C) and 85-95 MPa (at 35°C)
Tensile Strength, $\sigma_v$	24-27 MPa (at 15°C) and 26-31 MPa (at 35°C)
Shear Strength, $\tau$	14-17 MPa (at 15°C) and 16-19 MPa (at 35°C)

1

2 In order to ensure a perfect adhesion, the aluminium surface has been cleaned with acetone.

3

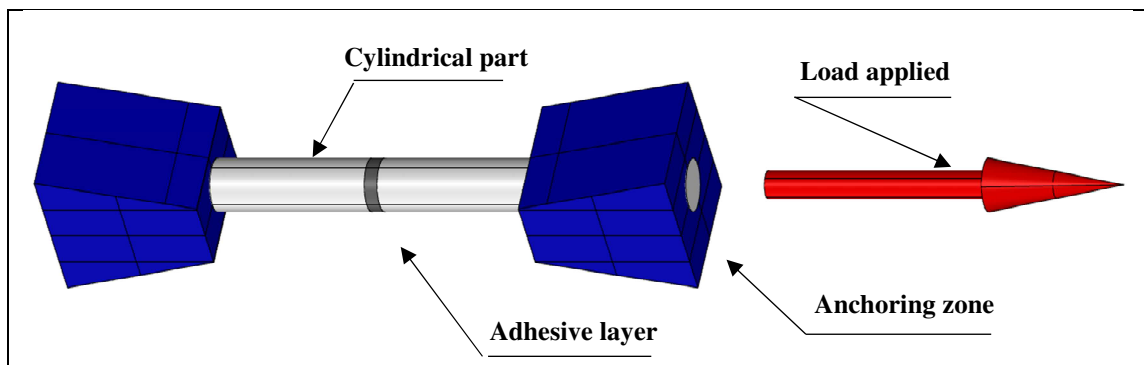


Fig. 8. – Cyclic Tests on adhesive cylindrical joint.

4

5 An aluminum device has been used to perform and control the thickness of adhesive desired and to  
 6 respect the coaxiality between the two aluminium half samples, in fact, the cylindrical part could slide  
 7 on it and have been fixed by means of two screws how depicted in Fig.9. Before to being tested, the  
 8 samples have been polymerized at room temperature for 7 days.

9

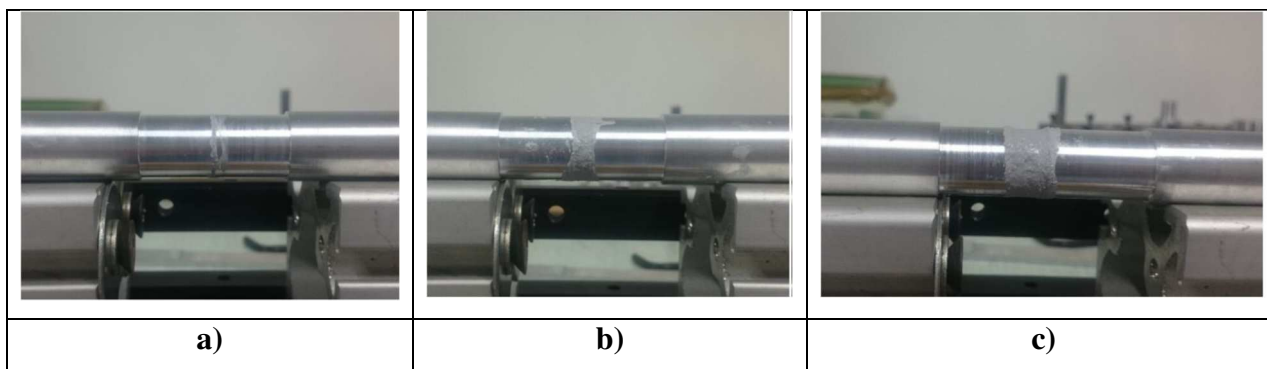


Fig. 9. Cylindrical specimens with different thickness of adhesive layer: a) 1 mm, b) 5 mm and c) 10mm.

10

11 The specimens were subject to high amplitude loading-unloading cyclic load by means of the traction-  
 12 compression machine “MTS 322 test frame” with a load capacity of 50 kN. The tests were performed  
 13 in displacement control at a rate of 1 mm/min.

14 The specimens, fixed at their ends, were tested according to an appropriate multistep up to failure  
 15 provoking an axial stress state, the main results for any thickness are collected in Table 3, 4 and 5.  
 16 Finally, the experimental curves stress vs time and stress vs displacement, recorded by the instrument,  
 17 are depicted as shown in the next section.

18

19

1  
2

**Table 3. Mechanical response of specimen At,1 in terms of displacement, stress and stiffness for any cycle (adhesive with 1 mm thickness)**

Cycle		$\delta_0$ [mm]	$\delta_1$ [mm]	$\sigma_0$ [Mpa]	$\sigma_1$ [Mpa]	$K_{exp}$ [N/mm <sup>3</sup> ]
1	loading	0.0030	0.0089	1.29	3.32	341
	unloading	0.0089	0.0000	3.32	0.43	324
2	loading	0.0000	0.0182	0.43	5.80	296
	unloading	0.0182	0.0000	5.80	0.07	315
3	loading	0.0000	0.0283	0.07	8.53	299
	unloading	0.0283	0.0000	8.53	0.03	301
4	loading	0.0000	0.0392	0.03	11.19	285
	unloading	0.0392	0.0004	11.19	0.50	276
5	loading	0.0004	0.0501	0.50	14.15	275
	unloading	0.0501	0.0001	14.15	0.16	280
6	loading	0.0001	0.0580	0.16	16.44	281
	unloading	0.0580	0.0008	16.44	0.50	279
7	loading	0.0008	0.0689	0.50	19.18	274
	unloading	0.0689	0.0009	19.18	0.04	281
8	loading	0.0009	0.0792	0.04	21.54	275
	unloading	0.0792	0.0019	21.54	0.05	278
9	loading	0.0019	0.0892	0.05	24.24	277
	unloading	0.0892	0.0038	24.24	0.39	279
10	loading	0.0038	0.0985	0.39	26.07	271
	unloading	-	-	-	-	-

3  
4  
5

**Table 4. Mechanical response of specimen At,5 in terms of displacement, stress and stiffness for any cycle (adhesive with 5 mm thickness)**

Cycle		$\delta_0$ [mm]	$\delta_1$ [mm]	$\sigma_0$ [Mpa]	$\sigma_1$ [Mpa]	$K_{exp}$ [N/mm <sup>3</sup> ]
1	loading	0.0019	0.0090	0.56	2.67	298
	unloading	0.0090	0.0011	2.67	0.51	275
2	loading	0.0011	0.0198	0.51	5.30	257
	unloading	0.0198	0.0003	5.30	0.30	258
3	loading	0.0003	0.0277	0.30	7.30	256
	unloading	0.0277	0.0016	7.30	0.29	269
4	loading	0.0016	0.0390	0.29	9.80	254
	unloading	0.0390	0.0010	9.80	0.18	253
5	loading	0.0010	0.0484	0.18	12.08	251
	unloading	0.0484	0.0012	12.08	0.37	249
6	loading	0.0012	0.0588	0.37	14.55	246
	unloading	0.0588	0.0033	14.55	0.41	255
7	loading	0.0033	0.0710	0.41	17.03	245
	unloading	0.0710	0.0031	17.03	0.04	250
8	loading	0.0031	0.0801	0.04	19.32	250
	unloading	0.0801	0.0031	19.32	0.10	249
9	loading	0.0031	0.0872	0.10	20.81	246
	unloading	0.0872	0.0061	20.81	0.31	253

10	loading	0.0061	0.0999	0.31	23.07	243
	unloading	0.0999	0.0697	23.07	15.34	256
11	loading	0.0057	0.1095	0.04	24.41	235
	unloading	0.1095	0.0086	24.41	0.16	240
12	loading	0.0086	0.1213	0.16	25.93	229
	unloading	0.1213	0.0144	25.93	0.16	241
13	loading	0.0144	0.1232	0.16	25.42	232
	unloading	-	-	-	-	-

**Table 5. Mechanical response of specimen At,10 in terms of displacement, stress and stiffness for any cycle (adhesive with 10 mm thickness)**

Cycle		$\delta_0$ [mm]	$\delta_1$ [mm]	$\sigma_0$ [Mpa]	$\sigma_1$ [Mpa]	$K_{exp}$ [N/mm <sup>3</sup> ]
1	loading	0.0028	0.0094	1.22	2.82	243
	unloading	0.0094	0.0003	2.82	0.30	275
2	loading	0.0003	0.0198	0.30	5.05	243
	unloading	0.0198	0.0002	5.05	0.21	247
3	loading	0.0002	0.0301	0.21	7.53	244
	unloading	0.0301	0.0003	7.53	0.16	246
4	loading	0.0003	0.0392	0.16	9.54	241
	unloading	0.0392	0.0000	9.54	0.20	238
5	loading	0.0000	0.0495	0.20	11.87	236
	unloading	0.0495	0.0003	11.87	0.29	235
6	loading	0.0003	0.0590	0.29	13.74	229
	unloading	0.0590	0.0012	13.74	0.16	235
7	loading	0.0012	0.0688	0.16	16.09	235
	unloading	0.0688	0.0006	16.09	0.04	235
8	loading	0.0006	0.0782	0.04	17.77	228
	unloading	0.0782	0.0026	17.77	0.35	230
9	loading	0.0026	0.0900	0.35	20.10	226
	unloading	0.0900	0.0016	20.10	0.27	224
10	loading	0.0016	0.0992	0.27	21.75	220
	unloading	0.0992	0.0028	21.75	0.20	224
11	loading	0.0028	0.1076	0.20	23.49	222
	unloading	0.1076	0.0047	23.49	0.35	225
12	loading	0.0047	0.1176	0.35	24.74	216
	unloading	-	-	-	-	-

In the table 3,4 and 5, the values of experimental tests are summarized in terms axial stress denoted by  $\sigma$ , subscripts 0 and 1 represent the initial and final point of loading/unloading curve;  $\delta$  represents the axial elongation of the glue evaluated by means of the results recorded. The amount of non-reversible elongation  $\delta_1$  at the end of the unloading steps is also analysed. The meaning of the symbols is summarized in Fig. 10.

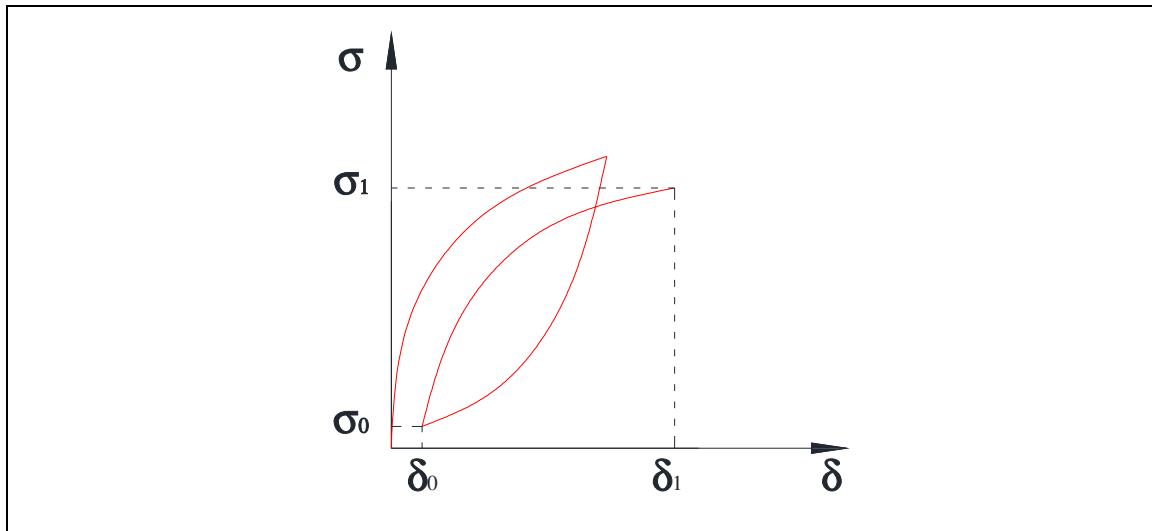


**Fig. 10. Typical stress-displacement experimental curve.**

1

2 The symbol  $K_{exp}$  indicates the experimental stiffness of the adhesive, evaluated over the generic step  
 3 by means of a linear fitting of the experimental data.

4 The experimental observation shows a slight decrease in the stiffness of the adhesive layer during the  
 5 loading cycles, which implies an increase in the initial damage due to microcrack propagation.  
 6 Furthermore, the results demonstrate that the mechanical properties of the adhesive layer are  
 7 influenced by the thickness. In particular, the increase of thickness of the adhesive layer leads to a  
 8 reduction of its normal strength and stiffness.

9 Finally, the description of damage parameters that take into account the presence of diffuse cracks,  
 10 are collected in Table 6. In particular, the initial damage length  $l_0$  have been evaluated by means of  
 11 Eqn. 6a. It is important to remark that the diffuse cracks present in the original adhesive layer can be  
 12 considered as a single large crack of length  $l$ .

13

14

**Table 6. Damage parameter in function of adhesive thickness**

Thickness ta (mm)	Initial damage length $l_0$ (mm)
1	11.44
5	12.33
10	12.96

15

16

17

18

19

20

21

## 5. Validation of the theoretical model

The imperfect model presented in Section 3, has been implemented in the commercial finite element software COMSOL Multiphysics. To assess the robustness and accuracy of the model, several simulations have been undertaken on the geometry of cylindrical specimens here presents, and of hollow column to built-up beam adhesive connections. Finally, comparisons between numerical and experimental results have been showed.

### 5.1. Comparison with cyclic tests on bonded cylinders

The cyclic behaviour has been investigated for all bonded cylinders experimentally tested at varying of adhesive layer thickness: 1,5 and 10 mm. Aluminium substrates are modelled by an isotropic linear elastic material which properties are reported in Table 1 while the mechanical properties of adhesive interface are reported in Table 2.

Due to the presence of two symmetry plane  $x-z$  and  $y-z$ , appropriate boundary conditions have been applied to model only un quarter of specimens optimizing the number of elements and the time of analysis.

The specimens have been fixed on the lower surface in the plane  $x-y$  reproducing the experimental test condition.

The numerical simulations have been undertaken both in displacement and force control. The displacement and force, function of time, have been applied on the upper surface of the cylindrical element along the vertical axis  $z$ . After a mesh sensitivity study on the elastic response of the interface, a number of 6340 3D tetrahedral elements have been chosen as depicted in Fig.11.

The numerical normal stiffness has been identified by comparison with experimental results and the damage parameter  $l_0$  evaluated by means of Eqn. 6.

The model parameters  $\bar{\eta}$  and  $\bar{\omega}$  have been calibrated from experimental data described in [13], where tensile static tests have been performed on adhesive bonded assemblies. In particular, the identification process of the two model parameters has been obtained comparing the global behavior of the simulated tests with the experimental one. It is worth to remark that the model parameters  $\bar{\eta} = 1.8e^9$  MPa and  $\bar{\omega} = -8e^4$  N/mm govern the post-peak behavior after the elastic limit and the energy threshold beyond which damage triggers, respectively.

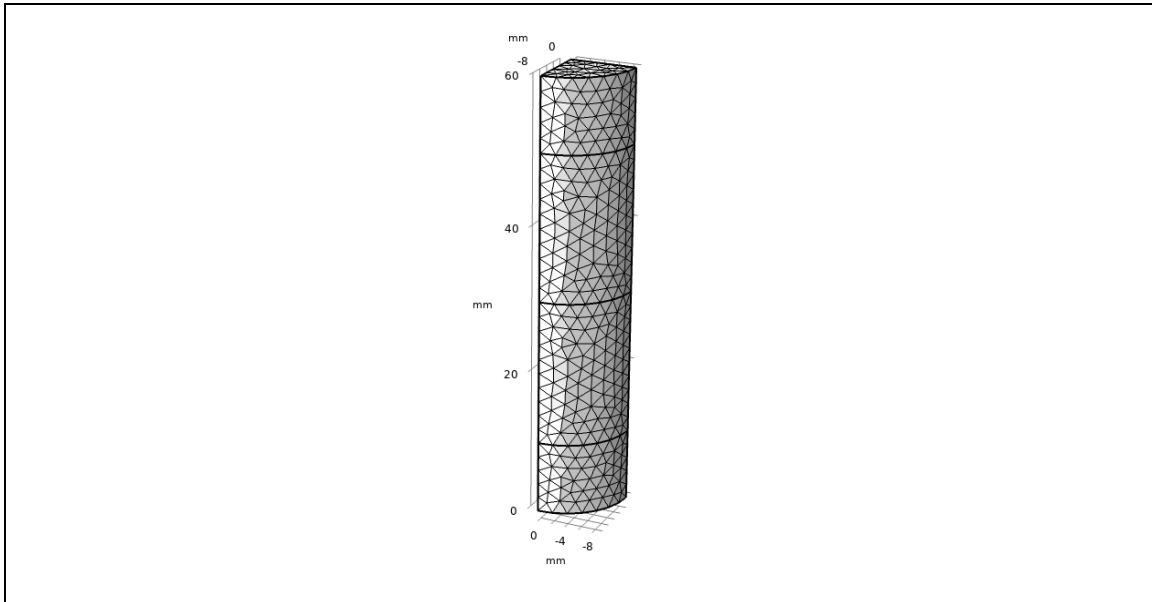


**Fig. 11. Mesh detail of cylindrical adhesive joint.**

1

2 Figs. 12 and 13 show for the bonded cylinder denoted At,1 (thickness of 1 mm) the computed and  
 3 corresponding experimentally measured stress-time relationship and stress-displacement curves.

4

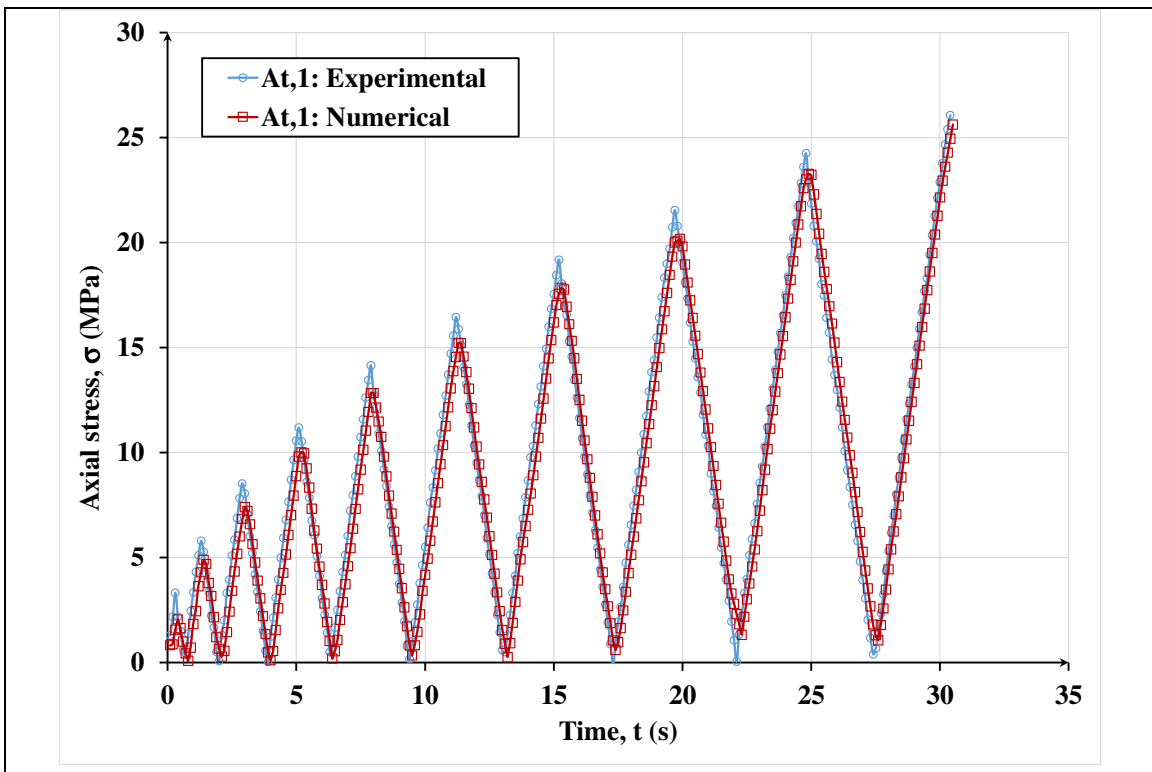


**Fig. 12. Comparison of computed and experimental stress-time curve for adhesive of 1 mm thickness (At,1).**

5

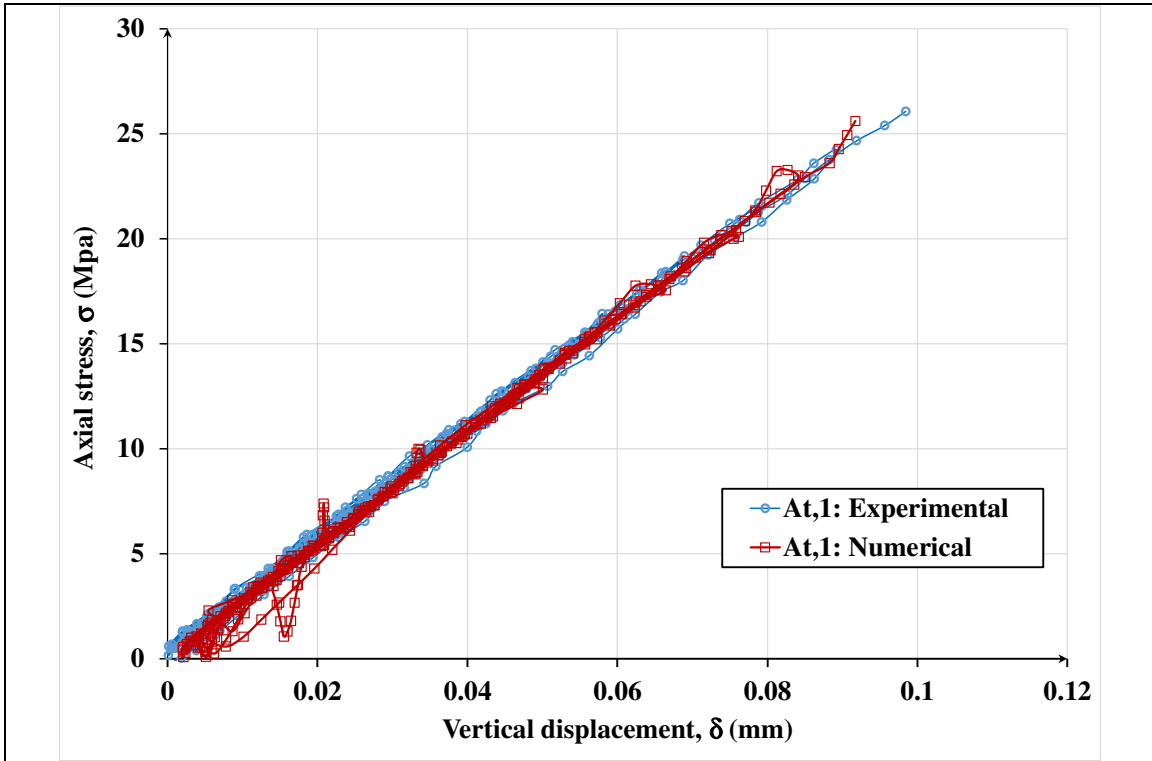


Fig. 13. Comparison of computed and experimental stress-displacement curve for adhesive of 1 mm thickness (At,1).

1

2 Figs. 14 and 15 show for the bonded cylinder denoted At,5 (thickness of 5 mm) the computed and  
 3 corresponding experimentally measured stress-time relationship and stress-displacement curves.

4

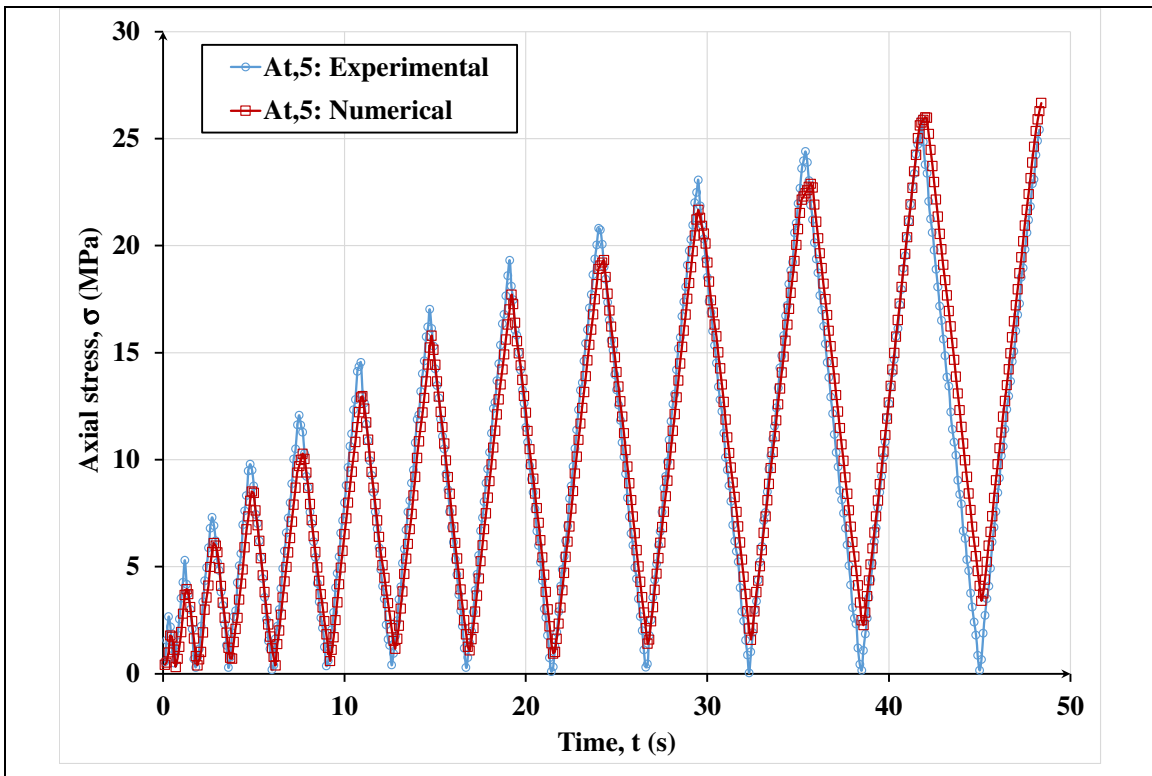
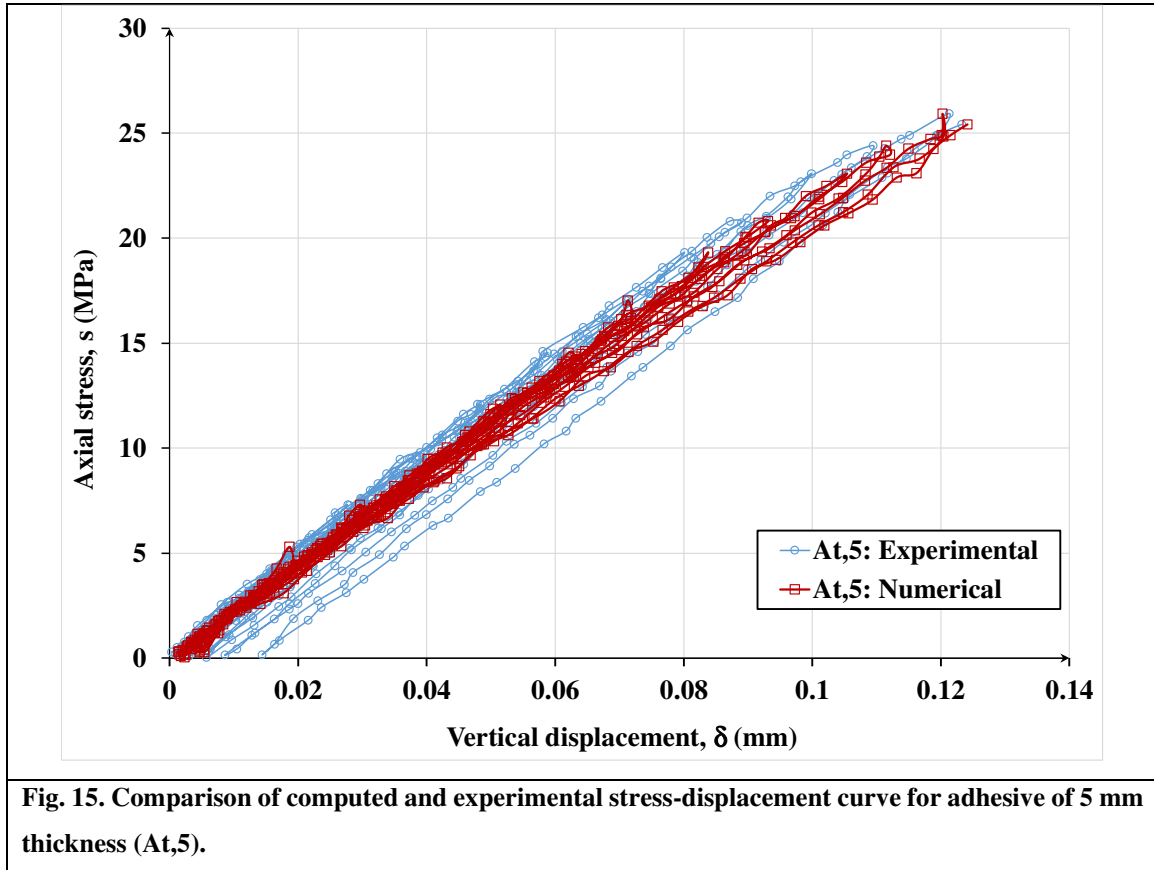


Fig. 14. Comparison of computed and experimental stress-time curve for adhesive of 5 mm thickness (At,5).

1  
2  
3



4  
5  
6  
7

Figs. 16 and 17 show for the bonded cylinder denoted At,10 (thickness of 10 mm) the computed and corresponding experimentally measured stress-time relationship and stress-displacement curves.

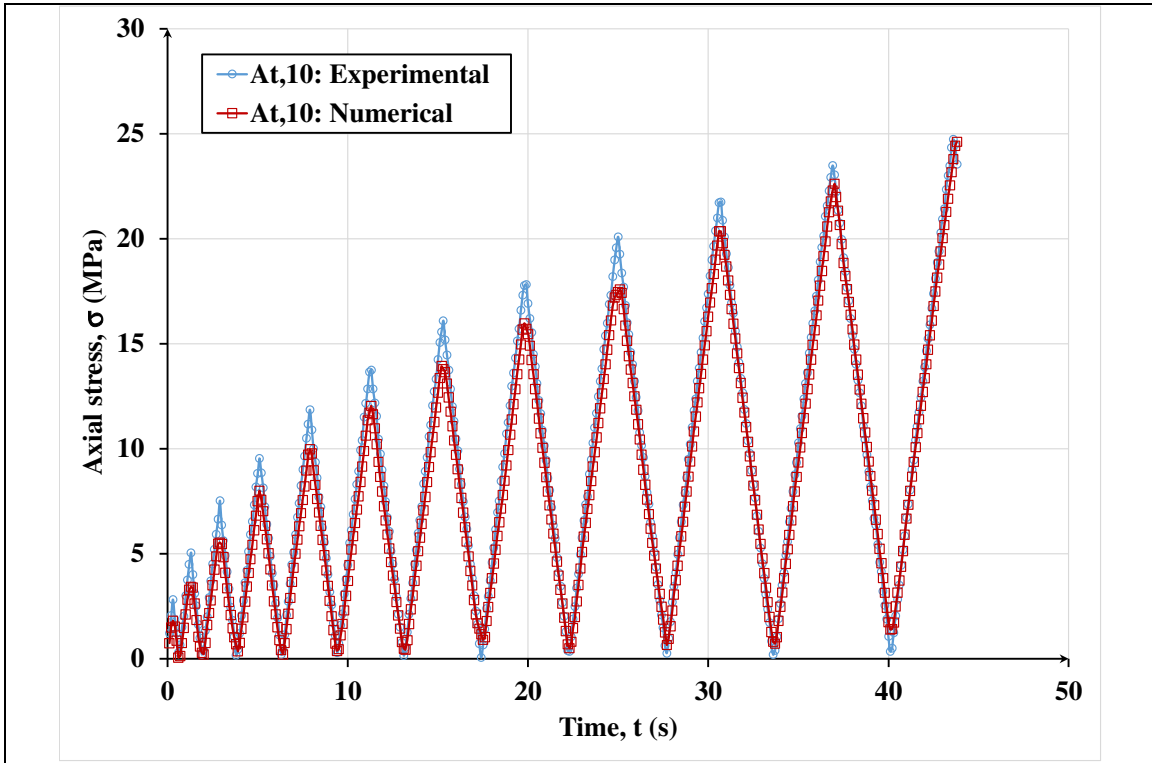


Fig. 16. Comparison of computed and experimental stress-time curve for adhesive of 10 mm thickness (At,10).

1

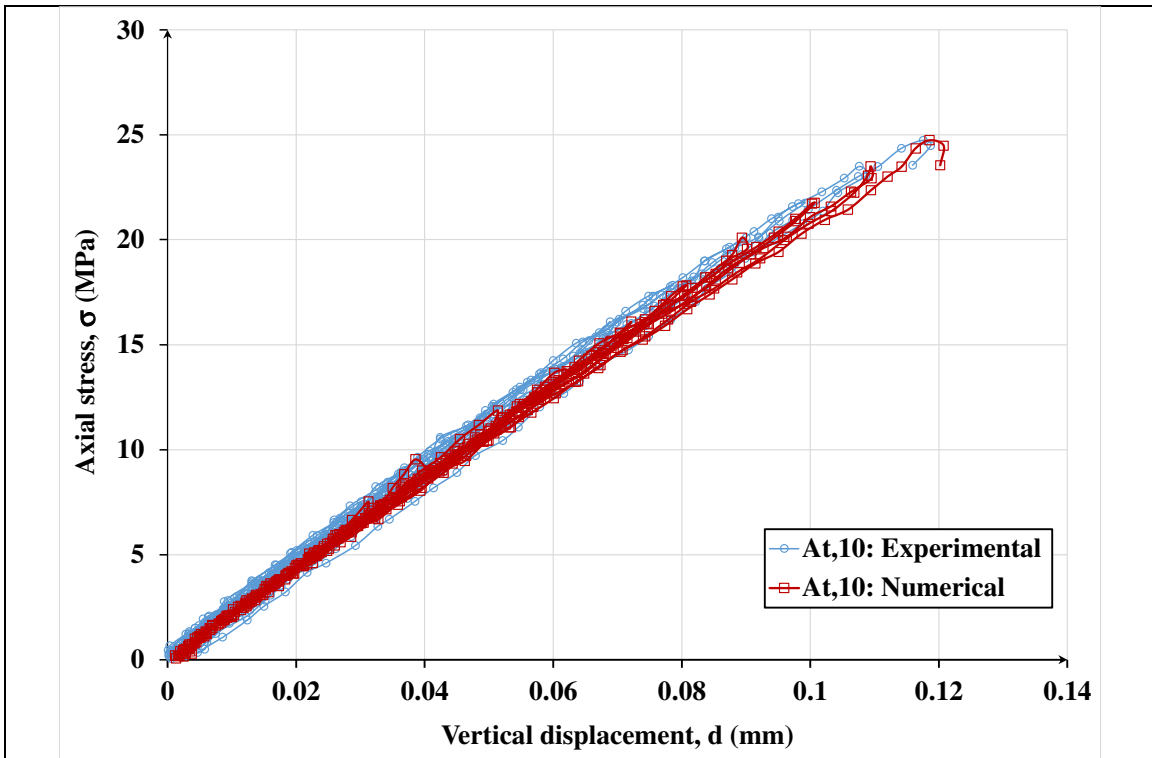


Fig. 17. Comparison of computed and experimental stress-displacement curve for adhesive of 10 mm thickness (At,10).

2

1 It is important to underline that the numerical results reported in Figs. 12, 14 and 16 have been  
2 obtained applying the load in displacement control and farther to highlighting the goodness of the  
3 model are able to show the load cycles applied to the samples.  
4 On the contrary, Figs. 13, 15 and 17 collect the numerical results in which the test procedure has been  
5 performed in force control.  
6 It is clear from the above comparisons that the imperfect model can accurately predict the above  
7 cyclic adhesive response at all loading stages up to their failure and the comparisons demonstrate the  
8 robustness and accuracy of the method.  
9 Finally, the evolution of the damage parameter  $l$  at varying of cycles load has been presented in Fig.  
10 18 for the test characterized by the presence of an adhesive layer of 10mm. It is important to underline  
11 that in the present model, the damage parameter that represents the average length of the cracks  
12 distributed inside the interface, grows as the number of cycles increases.  
13

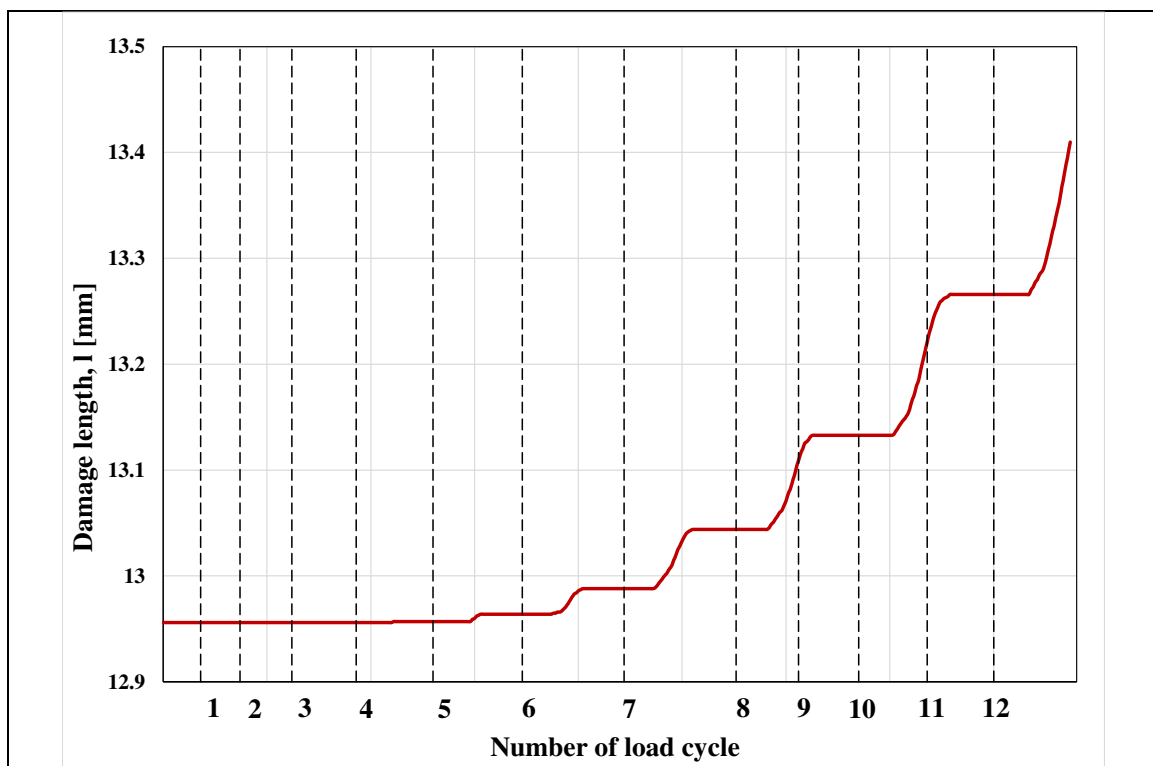


Fig. 18. Evolution of the damage parameter  $l$  (mm) at varying of number cycle.

14  
15 Finally, the graph depicted in Fig. 18 permitted to conclude that the evolution of the damage  
16 parameter  $l$  is strongly non-linear when an adhesive layer is subject to variable actions.  
17

## 18 5.2. Comparison with cyclic tests on GFRP hollow column to built-up beam adhesive connections

19  
20  
21 In order to demonstrate the capacity of the imperfect interface model to analyse the mechanical  
22 behaviour of complex adhesive structures, GFRP hollow column to built-up beam adhesive  
23 connections have been simulated using the COMSOL finite element package.

1 The GFRP material has been considered as transversally isotropic which mechanical properties are  
2 reported in Table 7.

3

4

**Table 7. Mechanical properties of GFRP pultruded laminates provided by the manufacturer.**

Mechanical properties		Value
Young's Modulus	$E_{0^\circ}$ [MPa]	23000
	$E_{90^\circ}$ [MPa]	8500
Shear Modulus	$G$ [MPa]	3000
Poisson's ratio	$\nu_{0^\circ}$	0.9
	$\nu_{90^\circ}$	0.23

5

6 The mesh of GFRP structures is described in Fig.19 consisting of 22550 3D tetraedric elements. The  
7 mesh has been refined in correspondence of the adhesive interface. The boundary conditions  
8 correspond to the test conditions: in fact, the column has been fixed at bottom and a displacement is  
9 applied at the same line where the load was imposed in the experimental tests.

10 It is important to underline that the damage evolution parameter  $l_0$  used in the current numerical  
11 investigation has been calibrated according to the experimental results ad hoc undertaken in the  
12 present research's work and before mentioned. The value of model parameters  $\bar{\eta} = 1e^9$  MPa and  $\bar{\omega}$   
13  $= -1e^5$  N/mm have been identified comparing the static global behavior of the simulated tests with the  
14 experimental results [11].

15

16

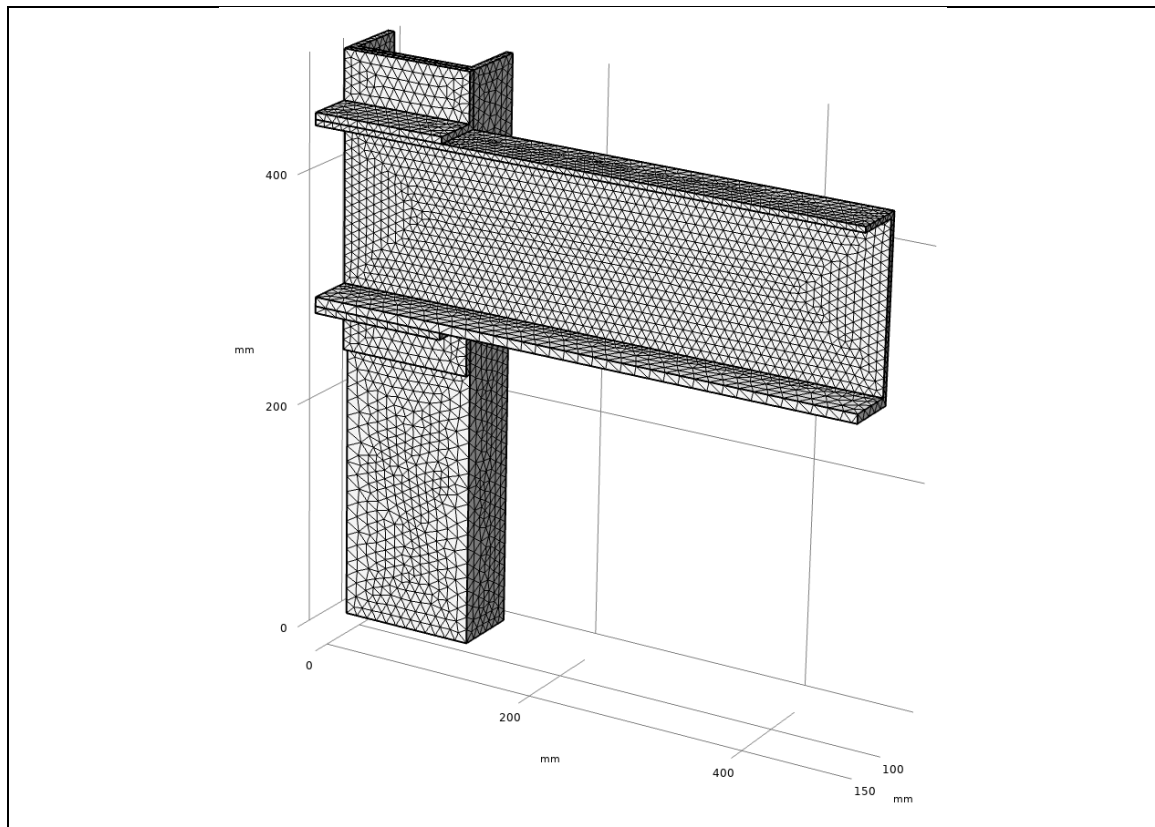


**Fig. 19. Mesh detail of GFRP hollow column to built-up beam adhesive connection.**

1  
2  
3  
4  
5

In Fig.20, the load versus the beam free end vertical displacement curve have been plotted and compare with the experimental results.

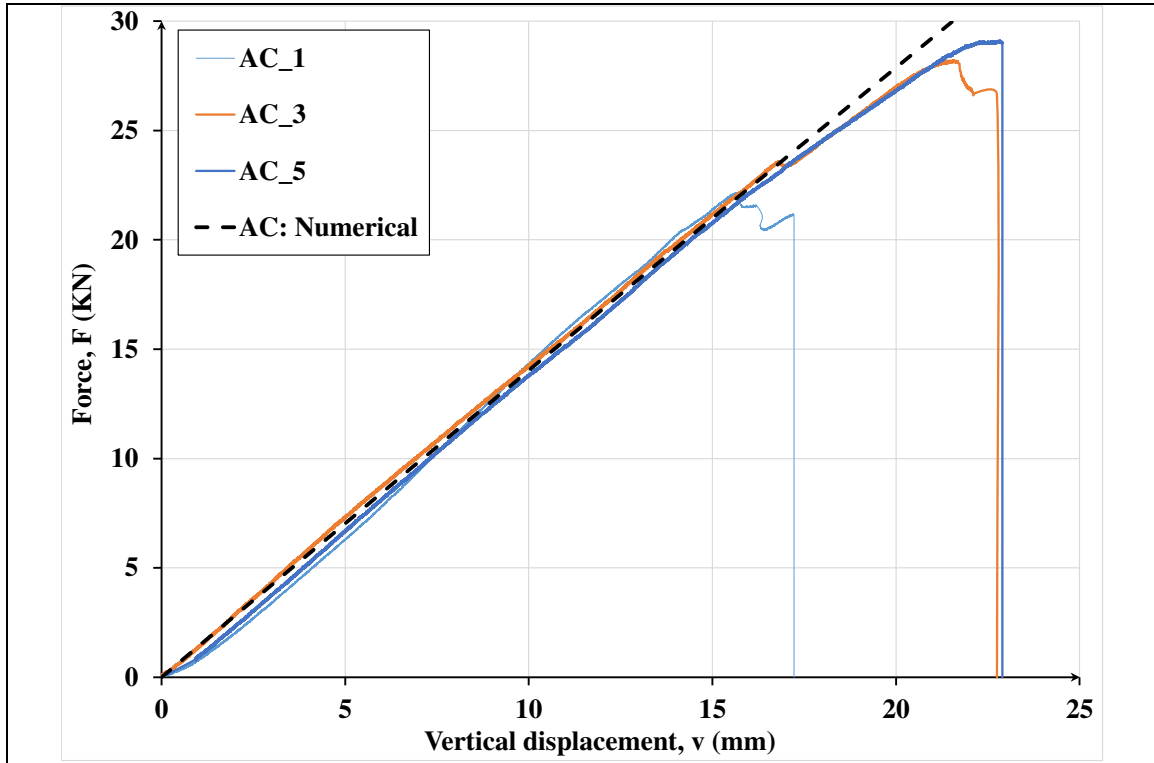


**Fig. 20. Comparison of computed and experimental force-displacement curve for GFRP hollow column to built-up beam adhesive connections.**

6  
7  
8  
9  
10  
11  
12  
13  
14  
15  
16  
17  
18  
19  
20

Furthermore, the comparison of computed and experimental force-displacement curve for GFRP hollow column to built-up beam adhesive connection (test denoted AC\_2) has been reported in Fig. 21. The specimen has been subjected to 400 cycles of equal load intensity. Finally, in Fig. 22 the comparison has been plotted with reference to the test denoted AC\_10. The specimen has been subject to four different groups of 60 cycles. The minimum load being 0.25 kN and the maximum loads for any group of cycles were 14, 21, 23.8 and 26.6 kN respectively.

1

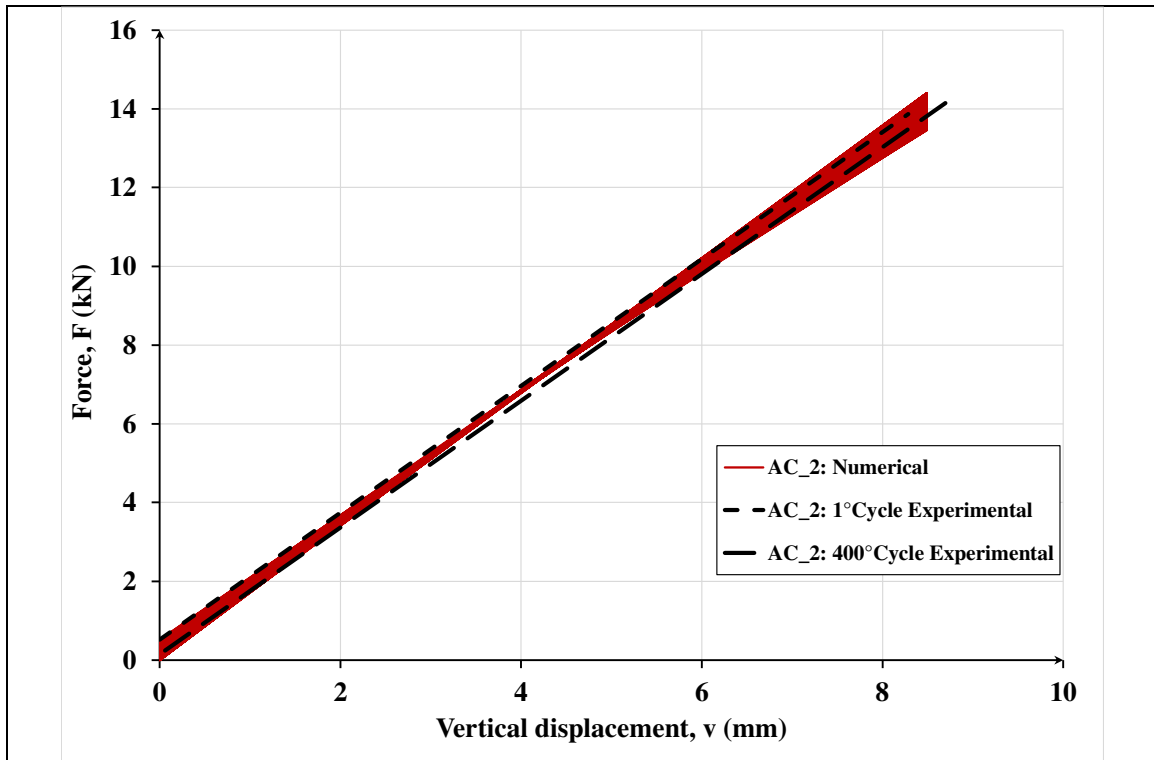
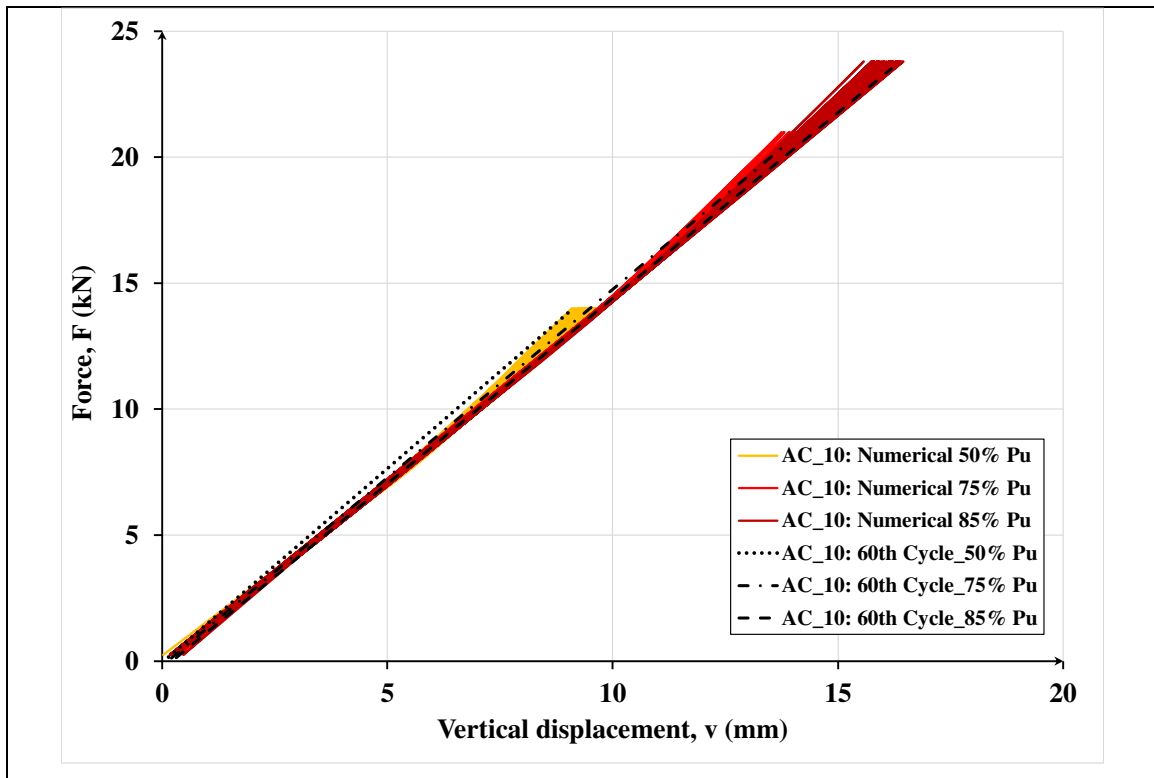


Fig. 21. Comparison of computed and experimental force-displacement curve for GFRP hollow column to built-up beam adhesive connection (test denoted AC\_2).

2

3



**Fig. 22. Comparison of computed and experimental force-displacement curve for GFRP hollow column to built-up beam adhesive connection (test denoted AC\_10).**

The good agreement underlines the capacity of the imperfect interface model proposed in this paper to simulate the static, cyclic and fatigue behaviour of complex adhesive structures. This lead to consider the imperfect interface model a powerful instrument able to describe the behaviour of adhesive joints stressed by variable intensity loads.

## 6. Conclusion

The cyclic behaviour of a structural adhesive available on the market has been evaluated by means of experimental tests performed on the universal testing machine. The parameter identified by the experimental evidence have permitted to model a GFRP hollow column to built-up beam adhesive connection under cyclic load by using an advanced imperfect interface model.

The results of the study support the following conclusions:

- 1) The thickness of adhesive layer influences the interface mechanical properties. In particular, the increment of thickness from 1 to 10 mm leads to a reduction of limit strength and a light reduction of stiffness as the number of load steps increases.
- 2) The experimental tests on the cylindrical specimens have permitted to calibrate the initial damage parameter  $l_0$  that depends on the thickness of the adhesive layer and of geometry of the bonded connections.
- 3) The numerical analysis highlighted that the evolution of damage parameter  $l$  is strongly non-linear in the presence of the adhesive connections subjected to cyclic and fatigue actions.
- 4) The successful strategy of associating an experimental procedure and a theoretical model provides a useful instrument for predicting the real behaviour of complex adhesive structures. The experimental and numerical analysis showed are in very good agreement establishing the powerful and robustness of the proposed model.

## Acknowledgement

This project has received funding from the European Union Horizon 2020 research and innovation programme under the Marie Skłodowska-Curie grant agreement No 843218-ASSO (Adhesive connection for Secondary Structures in Offshore wind installations).

## Data availability

The data required to reproduce these findings are all reported in the paper.

1  
2  
3  
4  
5  
6  
7  
8  
9  
10  
11  
12  
13  
14  
15  
16  
17  
18  
19  
20  
21  
22  
23  
24  
25  
26  
27  
28  
29  
30  
31  
32  
33  
34  
35  
36  
37  
38  
39  
40  
41  
42  
43

## 7. References

1. Correia JR. GFRP pultruded profiles in civil engineering: hybrid solutions, bonded connections and fire behaviour [PhD thesis in civil engineering] Instituto Superior Técnico, Technical University of Lisbon; 2008.
2. Carra G, Carvelli V. Long-term bending performance and service life prediction of pultruded glass fibre reinforced polymer composites. *Compos Constr* 2015;127:308–15.
3. Machado JJM, Marques EAS, da Silva LFM. Influence of low and high temperature on mixed adhesive joints under quasi-static and impact conditions. *Compos Constr* 2018;194:68–79.
4. Liao K, Schultheisz CR, Hunston DL. Effects of environmental aging on the properties of pultruded GFRP. *Compos B Eng* 1999;30(5):485–93.
5. Cabral-Fonseca S, Correia JR, Rodrigues MP, Branco FA. Artificial accelerated ageing of GFRP pultruded profiles made of polyester and vinylester resins: characterization of physical-chemical and mechanical damage. *Strain* 2012;48(2):162–73.
6. Fiberline Design Manual.
7. Report EUR 27666 EN. JRC Science for Policy Report, 2016.
8. Ascione F, Mancusi G, Spadea S, Lamberti M, Lebon F, Maurel-Pantel A. On the flexural behaviour of GFRP beams obtained by bonding simple panels: An experimental investigation. *Compos Struct* 2015;131:55–65.
9. Ascione F, Lamberti M, Razaqpur A, Spadea S. Strength and stiffness of adhesively bonded GFRP beam-column moment resisting connections. *Compos Struct* 2017;160:1248–57.
10. Ascione F, Lamberti M, Razaqpur A, Spadea S, Malagic M. Pseudo-ductile failure of adhesively joined GFRP beam-column connections: an experimental and numerical investigation. *Compos Struct* 2018;200:864–73.
11. Razaqpur AG, Ascione F, Lamberti M, Spadea S, Malagic M. GFRP hollow column to built-up beam adhesive connection: Mechanical behaviour under quasi-static, cyclic and fatigue loading. *Composite Structures*, 224, 111069 (2019).
12. Lamberti M, Maurel-Pantel M, Ascione F, Lebon F. Influence of web/flange reinforcement on the GFRP bonded beams mechanical response: a comparison with experimental results and a numerical prediction. *Compos Struct* 2016;147:247–59.
13. Maurel-Pantel A, Lamberti M, Raffa ML, Suarez C, Ascione F, Lebon F, “Modelling of a GFRP adhesive connection by an imperfect soft interface model with initial damage”, *Composite Structures* 2020: 239; 112034
14. Tsukrov I, Kachanov M. Effective moduli of an anisotropic material with elliptical holes of arbitrary orientational distribution. *Int J Solids Struct* 2000;69:5919–41.
15. Sevostianov I, Kachanov M. On some controversial issues in effective field approaches to the problem of the overall elastic properties. *Mech Mater* 2014;69:93–105.
16. SikaDur30 technical data sheet; 2020. URL:<http://fra.sika.com/dms/getdocument>.
17. Lebon F, Rizzoni R. Asymptotic behavior of a hard thin linear elastic interphase: an energy approach. *Int J Solids Struct* 2011;49:441–9.

- 1 18. Benveniste Y, Miloh T. Imperfect soft and stiff interfaces in two-dimensional elasticity. *Mech*  
2 *Mater* 2001;33(6):309–23.
- 3 19. Hashin Z. Thermoelastic properties of fiber composites with imperfect interface. *Mech Mater*  
4 1990;8(4):333–48.
- 5 20. Raffa ML, Lebon F, Rizzoni R. Derivation of a model of imperfect interface with finite strains  
6 and damage by asymptotic techniques: an application to masonry structures. *Meccanica*  
7 2018;53:1645–60.
- 8 21. Rekik A, Lebon F. Homogenization methods for interface modeling in damaged masonry.  
9 *Adv Eng Softw* 2012;46:35–42.
- 10 22. Bonetti E, Bonfanti G, Lebon F, Rizzoni R. A model of imperfect interface with damage.  
11 *Meccanica* 2017;52:1911–22.
- 12 23. Orefice A, Mancusi G, Dumont S, Lebon F. Experimental/numerical study on the interfacial  
13 damage of bonded joints for fibre-reinforced polymer profiles at service conditions.  
14 *Technologies* 2016;4. in line.

15  
16  
17  
18  
19  
20  
21